Am. J. Trop. Med. Hyg., 82(3), 2010, pp. 402–411
doi:10.4269/ajtmh.2010.09-0464

Design of Malaria Diagnostic Criteria for the Sysmex XE-2100 Hematology Analyzer

Germán Campuzano-Zuluaga,* Gonzalo Álvarez-Sánchez, Gloria Elcy Escobar-Gallo, Luz Marina Valencia-Zuluaga, Alexandra Marcela Ríos-Orrego, Adriana Pabón-Vidal, Andrés Felipe Miranda-Arboleda, Silvia Blair-Trujillo, and Germán Campuzano-Maya

Grupo Malaria, Faculty of Medicine, Universidad de Antioquia, Medellín, Colombia; Laboratorio Clínico Hematológico, Medellín, Colombia

Abstract. Thick film, the standard diagnostic procedure for malaria, is not always ordered promptly. A failsafe diagnostic strategy using an XE-2100 analyzer is proposed, and for this strategy, malaria diagnostic models for the XE-2100 were developed and tested for accuracy. Two hundred eighty-one samples were distributed into *Plasmodium vivax*, *P. falciparum*, and acute febrile syndrome groups for model construction. Model validation was performed using 60% of malaria cases and a composite control group of samples from AFS and healthy participants from endemic and non-endemic regions. For *P. vivax,* two observer-dependent models (accuracy = 95.3–96.9%), one non–observer-dependent model using built-in variables (accuracy = 94.7%), and one non–observer-dependent model using new and built-in variables (accuracy = 96.8%) were developed. For *P. falciparum,* two non–observer-dependent models (accuracies = 85% and 89%) were developed. These models could be used by health personnel or be integrated as a malaria alarm for the XE-2100 to prompt early malaria microscopic diagnosis.

INTRODUCTION

Early detection of malaria in patients not suspected of having the disease is a potential novel application for modern hematology analyzers like the Sysmex XE-2100 (Sysmex Corporation, Kobe, Kansai, Japan). A prompt and accurate diagnosis is critical to reduce adverse outcomes associated with malaria, including death.[1] In endemic regions, malaria is a prime diagnostic concern in febrile patients, and expert thick-film evaluation is usually available.[2] However, the accuracy of microscopic malaria diagnosis in less experienced centers or in non-endemic regions may be lower, and health personnel is less likely to consider the disease, leading to delayed diagnoses.[1] Automated full blood counts (FBC) are usually performed in patients with febrile illnesses, providing a unique opportunity to guide a timely parasitological malaria diagnosis.

Hematology analyzers evaluated for malaria detection include the Cell-Dyn (Abbott Diagnostics, Santa Clara, CA),[3] the GEN.S and LH-750 (Beckman Coulter, Miami, FL),[4] and the XE-2100 and XS-1000*i* (Sysmex Corporation, Kobe, Kansai, Japan).[5,6] The Sysmex XE-2100 is an automated hematology analyzer that uses flow cytometry, direct current (DC) impedanciometry, and radiofrequency conductance (RF) to detect and measure blood corpuscular elements.[7] Flow cytometry may detect malaria parasites or parasite debris such as free hemozoin or hemozoin-laden macrophages as reported for Cell-Dyn instruments.[8] For the Sysmex XE-2100, two case series reported a gap between the manual and automated eosinophil counts (pseudoeosinophilia) and abnormal granulocyte-coded events in the DIFF scatterplot used for white blood cell (WBC) separation based on fluorescence versus side-scatter signals in samples from *Plasmodium vivax*-infected patients.[9,10] Later, Huh and others[5] found that the two previously reported abnormalities, compared with thick film, had a sensitivity of 69.4% and a specificity of 100% for *P. vivax* diagnosis. These findings suggest the potential clinical utility of malaria detection by the XE-2100. Ideally, to improve the clinical impact of this detection method, it should be an automated process relying on the analyzer's quantitative data and expressed as a "malaria alarm" that could motivate the microscopic search for malaria.

The primary aim of this study was to develop, validate, and test the accuracy of one observer-dependent (OD) and two non–observer-dependent (N-OD) diagnostic prediction models for *P. vivax* and *P. falciparum* malaria. The approach for developing the OD models was similar to previous studies using the XE-2100 for malaria diagnosis[5] with the inclusion of other clinical and scatterplot variables not previously investigated. The N-OD models were developed to obtain a framework for an automated malaria-detection algorithm for the XE-2100. Secondary aims were to determine the occurrence of pseudoeosinophilia and to explore a possible cause for the XE-2100 FBC malaria-related abnormalities.

MATERIALS AND METHODS

Study population. Blood samples were collected from participants 13 years or older in the department of Antioquia, Colombia, South America from four malaria-endemic and one non-endemic municipality. Endemic municipalities were Necoclí (2,634 *P. vivax* cases/year; 246 *P. falciparum* cases/year) and Turbo (4,956 *P. vivax* cases/year; 705 *P. falciparum* cases/year) in the Urabá region and El Bagre (5,026 *P. vivax* cases/year; 1,724 *P. falciparum* cases/year) and Zaragoza (3,080 *P. vivax* cases/year; 443 *P. falciparum* cases/year) in El Bajo Cauca region.[11] Medellín, the non-endemic municipality, is an industrial city with no local cases of malaria.

Study design and predictive-model construction. We conducted a two-gate case-control diagnostic accuracy study where blood specimens were consecutively sampled into *P. vivax* or *P. falciparum* cases groups accordingly (Gates-1) and into two control groups (Gates-2a and 2b) as shown in Figure 1.[12] All the control group's samples were group-matched for age ± 6 years with the malaria group's samples. Participants who had taken anti-malarial drugs within 30 days were excluded. Samples from malaria (cases) and malaria-negative acute febrile syndrome (AFS controls, Gate 2a) groups were collected at the malaria-diagnosis services centers in the endemic regions and selected according to thick-film results (reference standard). The AFS group samples were from patients referred by local physicians for thick-film and FBC testing, and the definition for AFS was broad enough to include diseases clinically similar to malaria.

* Address correspondence to Germán Campuzano-Zuluaga, Laboratorio Clínico Hematológico, Carrera 43C No. 5-33, Medellín, Colombia 050022. E-mail: germancz81@gmail.com

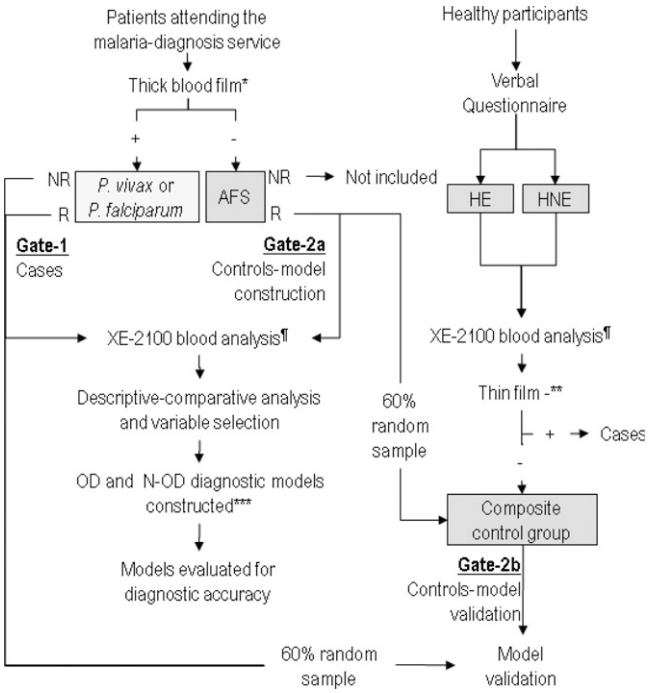

FIGURE 1. Study design and sampling procedure. R, referred by physician; NR, not referred by physician; AFS, participant with malaria-negative acute febrile syndrome; HE, healthy participant from endemic region; HNE, healthy participant from non-endemic region. Details in text. *Diagnostic reference standard for malaria versus AFS. **Diagnostic reference standard for malaria versus healthy in composite control. ***Index test diagnostic criterion (optimal predicted probability obtained for each diagnostic model). ¶Blood analysis from where data were obtained to construct the index diagnostic criteria.

Whole blood from all participants was processed in a XE-2100 analyzer, and the quantitative data, scatterplots, and histograms obtained were used to construct predictive models (index tests) for each malaria species using binary logistic regression (LnR). The dependent variable was malaria status (positive = *P. vivax* or *P. falciparum*; negative = AFS), and the independent variables were those obtained from the XE-2100 analyses. Sample size was estimated as $N = 10(k + 1)$, where k is the number of independent variables in each LnR model.[13] The variables modeled were selected based on bivariate comparisons between malaria and AFS groups (Mann–Whitney's U and Student's t test for continuous data and χ^2 test for categorical data; inclusion criteria was $P < 0.25$), univariate LnR analyses (inclusion criteria was $P < 0.25$), and correlation analyses (Spearman's and Kendall's coefficients; $r < 0.6$). The models were built stepwise with forward-Wald P value of 0.1 as criterion for exclusion of variables from the model. Strength-of-association (Nagelkerke's R^2) test, goodness-of-fit (Pearson's χ^2 and Hosmer–Lemeshow statistic) tests, and the models accuracy were considered for selection of the final models for each malaria species. The predicted probability (PP) for malaria given by the formula,

$$PP(malaria) = \frac{1}{1 + e^{-(\beta_0 + \beta_1 x_1 + \beta_2 x_2 + \ldots + \beta_n x_n)}}$$

(β_0, intercept; $\beta_{1,2,\ldots n}$, fitted coefficients; $x_{1,2,\ldots n}$, variable values) was obtained from each model and calculated for each sample. The discrimination accuracy and optimal cut-off PP of each model was determined using receiver-operating characteristic (ROC) curve analysis. The index test diagnostic criteria were defined as the optimal malaria PP obtained for each model (positive: ≥ optimal PP; negative: < optimal PP) and were tested for sensitivity, specificity, likelihood ratios and Youden's J against the reference standard (microscopy). Confounding was assessed for sex, age (in deciles), ethnicity, and time to process the sample. The prediction models developed were the following: one univariate (U-OD) and one multivariate (M-OD) observer-dependent model for *P. vivax* that included visually assessed categorical variables (presence or absence of abnormalities) from the XE-2100 graphical analyses (Figure 2). With the M-OD$_{P.\ vivax\ (Pv)}$ model, an integer-point Malaria$_{Pv}$ Score was obtained by dividing the fitted coefficients (β_n) by the smallest coefficient and rounding the quotients to the nearest integer. For both *Plasmodium* species, one N-OD model using the analyzer's built-in variables (clinical and technical; N-OD1) and one N-OD model using the built-in variables and pixel counts in scatterplot areas not registered by the commercial XE-2100 Information Processing Unit (IPU; N-OD2) were built. N-OD models were modeled using their original scale, because they were designed to be computed by a laboratory information system (LIS).

The models were cross-validated comparing a random 60% sample of the malaria cases with a composite control group (controls validation is Gate 2b) that consisted of a random 60% sample of the AFS group, samples from healthy companions from an endemic region (HE), and samples from healthy participants from a non-endemic region (HNE; Figure 1). Healthy was defined as an asymptomatic participant with no history of malaria in the previous 2 months and a malaria-negative thin film (reference standard). The study was approved by the Ethics Committee of the Sede de Investigación Universitaria of the Universidad de Antioquia, and all participants signed a consent before enrolling the study.

Secondary analyses. The gap between the manual and automated differential WBC counts [neutrophils, eosinophils (pseudoeosinophilia), basophils, lymphocytes, and monocytes] was defined as [(automated WBC count – manual WBC count)/automated WBC count] × 100. To explore the possible cause of the XE-2100 malaria-related abnormalities, linear and logistic regression analyses were performed with the FBC variables as dependent variables and the differential parasitemias (rings, mature trophozoites, schizonts, and gametocytes) as independent variables.

Data recollection, diagnostic procedures, and laboratory studies. As the reference diagnostic test, duplicate thick films from patients attending the malaria-diagnosis service were dyed with Field's stain and read by one experienced field microscopist and one experienced laboratory microscopist; a third examiner resolved discrepancies. Two-hundred high-power fields were evaluated before excluding malaria, and species was determined morphologically.[14] Total and differential parasite counts were done per 200 WBCs and converted to terms of the automated WBC count to parasites per microliter. For the index test, whole blood was collected in 4-mL, dipotassium ethylene diamine tetraacetic acid containing Vacutainer tubes (Becton, Dickinson and Company, Franklin Lakes, NJ) and transported at ≈10°C to Medellín within the sample viability range (36 hours).[7,15] Two-hundred microliters of blood were processed in a commercial Sysmex XE-2100 (Sysmex Corporation, Kobe, Kansai, Japan). This

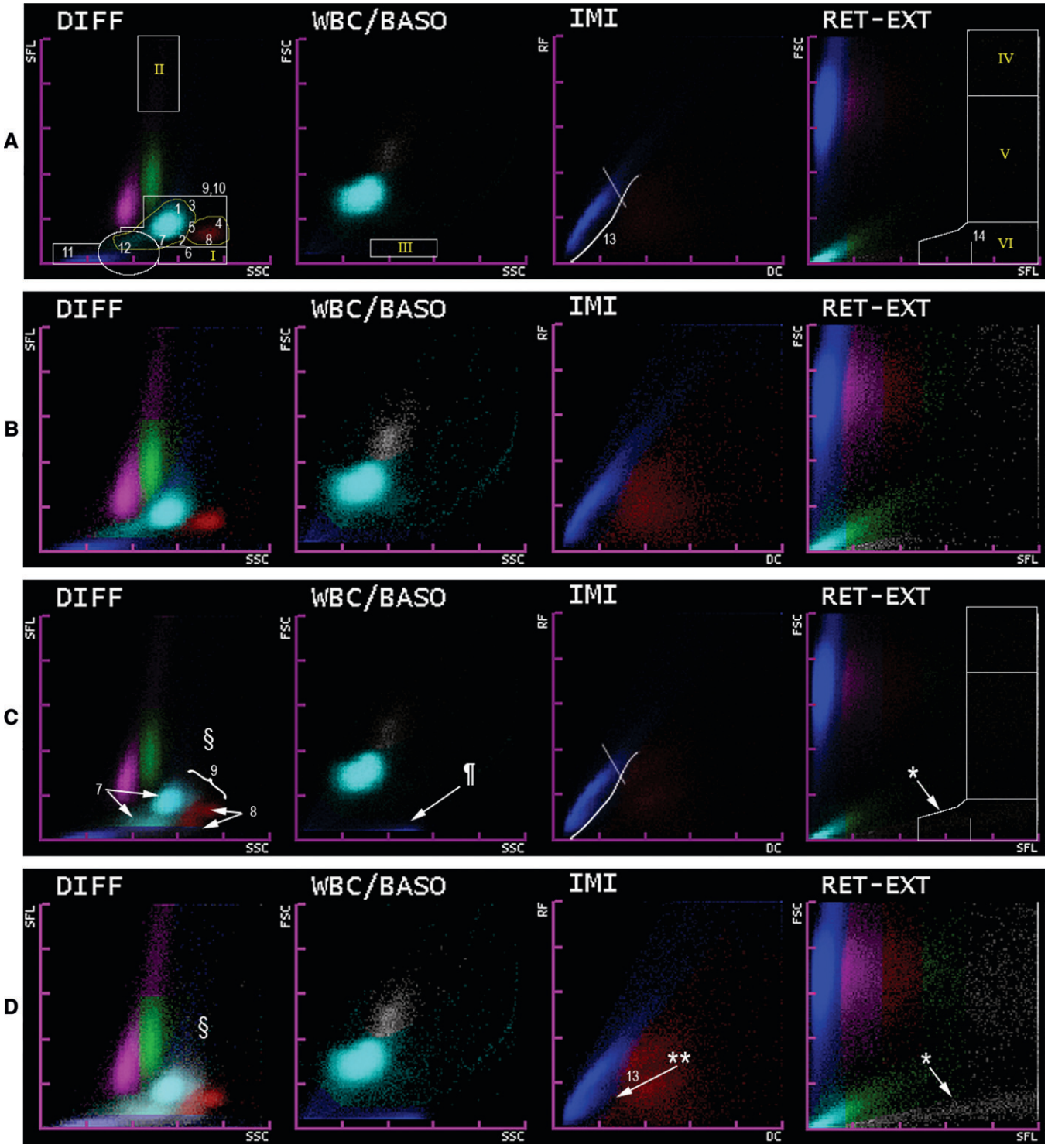

FIGURE 2. Summary images and level-edited summary images obtained using Photoshop CS3 for AFS (**A** and **B**) and *P. vivax* (**C** and **D**). White and yellow perimeter lines in **A** delimit the areas where scatterplot variables not given by the XE-2100 IPU where codified for analysis (Supplementary Panel 1). **C** depicts the general XE-2100 *P. vivax* pattern. Arabic numerals correspond to categorical variables: 1, neutrophil group, outside limit (yellow line); 2, neutrophil group, inferior deviation; 3, neutrophil group, right deviation; 4, eosinophil group, outside limit (yellow line); 5, confluent neutrophil and eosinophil groups; 6, granulocyte-coded events outside inferior limit; 7, number of neutrophil-coded group(s) (1 or 2); 8, number of eosinophil coded group(s) (1 or 2); 9, tendency of granulocytes to form one group; 10, abnormal granulocyte-coded group color (gray or normal); 11, gray RBC ghosts; 12, fusion of neutrophil group and RBC ghosts; 13, WBC blue group crosses limiting line; 14, high SFL gray events past limiting line. Variables 1–10 conform to the compound **variable number of granulocyte-coded DIFF abnormalities**. Roman numerals correspond to pixel counting areas [DIFF(I), DIFF(II), WBC/BASO(III), RET-EXT(IV), RET-EXT(V) and RET-EXT(VI))]. §**C** and **D** show the duplication (arrows) of neutrophil and eosinophil groups in the DIFF scatterplot and the fusion (bracket) of all granulocyte-coded events. ¶Abnormal events in the WBC/BASO(III) counting area. **The wide IMI WBC ghost group. *The alinear pattern of fluorescent gray-coded events revealed in the level-edited summary image.

analyzer measures 32 clinical and 115 technical variables of which we studied 45 built-in (28 clinical and 17 technical) quantitative variables [6 red blood cell (RBC), 6 reticulocyte, 8 WBC, 9 platelet (PLT), and 16 scatterplot variables listed in Supplementary Table 2, available at www.ajtmh.org]. The XE-2100 uses DC to generate PLT and RBC histograms, DC and RF to detect immature WBC (IMI scatterplot), and semiconductor laser-light 90° side-scatter (SSC) and 0° forward-scatter (FSC) and polymethyne 90° side-fluorescence (SFL) to generate six scatterplots that separate WBCs (DIFF and WBC/BASO scatterplots), nucleated red blood cells (NRBC scatterplot), and RBCs and PLTs (RET-EXT, RET, and PLT-O scatterplots; Figure 2 and Supplementary Figure 1, available at www.ajtmh.org).[15–17] This study analyzed the DIFF, WBC/BASO, IMI, NRBC, and RET-EXT scatterplots. The mean SSC, FSC, and SFL values (given in arbitrary units by the manufacturer) in each scatterplot axis (*X* and *Y*) for each cell type were available as technical variables. Thin films prepared by a Sysmex SP-1000*i* were used for manual WBC differentials and parasite search in the HE and HNE group samples.

XE-2100 graphical analysis. The commercial XE-2100 IPU is not programmable for scatterplot analyses different from those specified by the manufacturer. To analyze several malaria-related scatterplot abnormalities not reported by the IPU that were required for the OD and N-OD2 models, they were edited and analyzed using Photoshop CS3 v10.0 (Adobe Systems Incorporated 1990–2007, San Jose, CA; Figure 2). A detailed explanation of the editing and analysis procedure can be found in Supplementary Panel 1 (available at www.ajtmh.org). Briefly, variables were established in three steps. First, in an open evaluation of 208 random images of all groups, areas with malaria-related patterns or events (pixels) were grossly identified. Second, to finely limit these areas, summary images were created by superposing 50 random images, each with fill (transparency) value of 2%, to obtain a compound image with fill value of 100% for each group. Third, a level-edited summary image, where middle tones were overexposed, was created to reveal pixels unlikely to superpose in the summary images as in the RET-EXT scatterplot (Figure 2C and D). The delimited malaria-related patterns were then codified as observer-dependent categorical (presence or absence of pattern) or pixel-count quantitative variables (command, image analysis: histogram: quantity).[18] Ten abnormalities in the granulocyte area in the DIFF scatterplot were summed in a variable denoted as **number of granulocyte-coded DIFF abnormalities** (Figure 2). Categorical variables were evaluated in three interrater and intrarater analyses with researchers masked to the study group and to the other researcher's results. A final set of 14 reproducible categorical variables (kappa coefficients > 0.6)[19] and six pixel-count variables were obtained and also evaluated in a masked procedure for all samples (Supplementary Tables 1 and 2, available at www.ajtmh.org).

Statistical analysis. Data were analyzed with SPSS v17 (SPSS Inc. 2008, Chicago, IL) and Epidat v3.1 (EPIDAT 2005, *Xunta de Galicia*, Santiago de Compostela A Coruña, Spain; PAHO, Unit of Health Analysis and Information Systems, Washington, DC). Statistical significance was set at ≤ 0.05, and 95% confidence intervals (95% CI) were obtained for diagnostic accuracy estimates.

RESULTS

A total of 281 blood samples were collected between November 2008 and February 2009. Median age, sex, and time to process the samples was similar between study groups (Table 1). In the AFS group, 57% of the patients were diagnosed with unspecific febrile syndromes, 21% with upper respiratory infection, 9% with gastroenteritis, 6% with lower respiratory infection, 3% with urinary tract infection, 2% with dengue fever, and 2% with primary varicella infection. One patient was reallocated from the AFS to the *P. falciparum* group after visualizing ring forms in the duplicate thick-film evaluation.

XE-2100 variables among study groups. Bivariate comparisons and univariate LnR analyses of the FBC variables between each malaria group and the AFS group are shown in Supplementary Table 1. Briefly, there was a significant decrease in the RBC and PLT counts and an increase in RBC and PLT volume distributions in both malaria groups. Reticulocyte counts were significantly higher in both malaria groups, but the reticulocyte-count/immature-reticulocyte fraction (IRF) ratio was similar between groups. There were significant differences in the scatterplot mean *X* and *Y* axis values for lymphocytes (LYMPH-Y and LYMPH-X) and immature WBCs (IMI-DC and IMI-RF) in both malaria groups, in the WBC DIFF channel (DIFF-Y), NRBCs (NRBC-X), and reticulocytes (RET-X) for *P. vivax*, and in the NRBC-Y and the RBC channels (RBC-X, and RBC-Y) for *P. falciparum.* The ratio between the DIFF WBC count and the total WBC count (ΔDIFF/WBC) was significantly higher for *P. vivax*. The proportion difference for thrombocytopenia (PLT < $150 \times 10^3/\mu L$) between *P. vivax* and AFS was 65.5% (95% CI = 52.4–79.6%) and between *P. falciparum* and AFS was

TABLE 1
Descriptive statistics of participants and samples

Variable	Total *N = 281*	Cases (Gate 1)		Controls	
		P. vivax N = 65	*P. falciparum N = 30*	AFS (Gate 2a) *N = 63*	Composite* (Gate 2b) *N = 161*
Females % (*n*)	39.9 (112)	40 (26)	47 (14)	40 (25)	38.5 (62)
Median age in years (IQR)	25 (19–35)	22 (17–29)	28 (20–44)	29 (18–37)	25 (19–37)
Rural residence % (*n*)	49.5 (139)	86 (56)	97 (29)	52 (33)	26.7 (43)
Ethnicity % (*n*)					
Afro-Colombian	14.6 (41)	12 (8)	20 (6)	19 (12)	13.7 (22)
Indigenous	1.1 (3)	0	0	2 (1)	1.9 (3)
Mestizo	72.2 (203)	65 (42)	67 (20)	68 (43)	77.6 (125)
White	3.9 (11)	9 (6)	0 (0)	6 (4)	1.2 (2)
ND	8.2 (23)	14 (9)	13 (4)	5 (3)	5.6 (9)
Median time in hours to process sample (IQR)	26:54 (23:59–29:56)	25:02 (22:40–28:14)	24:09 (23:43–26:34)	29:19 (24:46–31:02)	27:57 (25:09–30.29)

*Composite control includes samples from AFS (*N* = 39), HE (*N* = 56), and HNE (*N* = 67) groups. IQR = interquartile range; ND = no data available.

39% (95% CI = 19–60%). The proportion difference for anemia (hemoglobin < 12 mg/dL) between *P. vivax* and AFS was 13.2% (95% CI = –2.0–28.4%) and between *P. falciparum* and AFS was 22% (95% CI = 2–43%).

XE-2100 graphical output analyses. Representative scatterplots of the AFS, *P. vivax*, and *P. falciparum* groups are shown in Figure 3. A general XE-2100 *P. vivax* pattern was observed in the DIFF, WBC/BASO, IMI, and RET-EXT scatterplots (Figures 2 and 3) and was fractioned into 14 categorical variables (Arabic numerals in Figure 2 and Supplementary Table 1) and 6 pixel-counting areas (Roman numerals in Figure 2 and Supplementary Table 2). The WBC ghost group in the IMI scatterplots showed a rightward shift in samples with *P. vivax*, and no important abnormalities appeared in the NRBC scatterplots. The interrater and intrarater kappa coefficients for the XE-2100 *P. vivax* pattern variable were 0.92 (95% CI = 0.83–1.00) and 0.96 (95% CI = 0.87–1.00), respectively (Supplementary Table 1). In the *P. vivax* group, 98% had ≥ 1 of 10 possible abnormalities for the variable number of granulocyte-coded DIFF abnormalities compared with 36% in the AFS group ($P < 0.001$; Figure 2). The only *P. falciparum* sample with an abnormal scatterplot consisting of a second eosinophil-coded group in the DIFF scatterplot also had the highest gametocytemia (1,613 gametocytes/μL versus group mode; 0 gametocytes/μL). PLT and RBC histograms showed extra peaks in both malaria groups but had low reproducibility (kappa of 0.55 and 0.36, respectively) and were not included in further analyses (Supplementary Figure 2, available at www.ajtmh.org). Compared with the AFS group, pixel counts were significantly higher in all six counting areas, except the RET-EXT(IV) for *P. vivax*, and in none of the RET-EXT areas for *P. falciparum* (Figure 2; Supplementary Table 2). Optimal cut-off values and diagnostic accuracy of pixel counts are shown in Table 2.

Diagnostic models. Four *P. vivax* and two *P. falciparum* prediction models were constructed. Model characteristics with variables included, strength of association, regression coefficients, diagnostic odds ratios (DOR), optimal cut-off PPs, diagnostic accuracy, and validation results are shown in Tables 3 and 4, Supplementary Panel 2 (available at www.ajtmh.org), and described as follows. Differences in sex, age, ethnicity, and time to process the samples did not significantly alter the regression coefficients of the variables selected for the models.

P. vivax diagnostic models. One univariate and one multivariate OD *P. vivax* diagnostic model was obtained ($N = 128$). The univariate OD_{Pv} (U-OD_{Pv}) model consisted in the recognition of the general XE-2100 *P. vivax* pattern. A $Malaria_{Pv}$ Score constructed from the multivariate OD_{Pv} (M-OD_{Pv}) model consisted of 11 variables that were ≥ 7 pixels in the WBC/BASO(III) (3 points) and the number of granulocyte-coded DIFF abnormalities (10 variables; 1 point per variable) with ≥ 4 points achieving the optimal accuracy (Tables 3 and 4; Figure 2; Supplementary Figure 3, available at www.ajtmh.org). The N-$OD1_{Pv}$ ($N = 114$) model included the continuous decrease in 1% units of plaquetocrit, the continuous increment in the ΔDIFF/WBC, and the continuous increase in mean *Y* axis units of lymphocyte-coded events (LYMPH-Y). The increase in LYMPH-Y had a small but significant correlation with the pixel count in DIFF(II) ($R^2 = 0.045$; $P < 0.001$), and the increase in ΔDIFF/WBC showed a significant correlation with the number of granulocyte-coded DIFF abnormalities ($R^2 = 0.318$; $P < 0.001$). The N-$OD2_{Pv}$ ($N = 128$) model included the continuous increase in the WBC/BASO(III) pixel count and the continuous decrease in optic platelet count ($\times 10^3$/μL; PLT-O).

P. falciparum diagnostic models. OD models could not be developed for the *P. falciparum* group because of the lack of significant scatterplot abnormalities. The *P. falciparum* N-$OD1_{Pf}$ ($N = 91$) model included the continuous increase in red cell distribution width (RDW-SD) in femtoliters, the continuous decrease in the PLT-O count, and the continuous increase in LYMPH-Y. The N-$OD2_{Pf}$ ($N = 91$) model included an increase in RDW-SD, the continuous decrease in the PLT-O count, and the continuous increase of pixels in the WBC/BASO(III) scatterplot.

Manual and automated WBC differential counts. A median pseudoeosinophilia of 33.9% (interquartile range [IQR] 94) was found in the *P. vivax* group compared with 5.6% (IQR 140) in the AFS group ($N = 114$; $P = 0.16$). The optimal pseudoeosinophilia for *P. vivax* diagnosis was 20.9% (ROC area under the curve [AUC] = 0.575; $P = 0.17$). No pseudoeosinophilia was found in the *P. falciparum* group. The lymphocyte, monocyte, and neutrophil counts showed no significant gaps for any of the malaria groups.

Parasitemia and associations with FBC variables. Differential parasite counts are shown in Supplementary Table 3 (available at www.ajtmh.org). The sample with the lowest *P. vivax* parasitemia (190 parasites/μL containing 76 mature trophozoites/μL and 114 schizonts/μL) was detected by both N-OD_{Pv} models but neither OD_{Pv} models. The sample with the lowest *P. falciparum* parasitemia (356 parasites/μL; 32 gametocytes/μL) was detected by both N-OD_{Pf} models. Significant associations between the XE-2100 abnormalities and the differential parasite counts are shown in Table 5 and Supplementary Table 4 (available at www.ajtmh.org). *P. vivax* mature trophozoites and schizonts showed a strong and significant association with abnormalities in the DIFF, WBC/BASO, and RET-EXT scatterplots followed by gametocytes and rings. The ΔDIFF/WBC was associated with the presence of *P. vivax* mature trophozoites, and for both species, ring forms were associated with an increase in LYMPH-Y. No significant associations were found for platelet or RDW-SD measurements.

DISCUSSION

There is substantial evidence that modern hematology analyzers can detect malaria-associated events, mostly by interference with the flow cytometry[20] and DC measurements.[21] Three prototypes of analyzers have been evaluated for malaria diagnosis. The Cell-Dyn analyzers detect monocyte-coded depolarizing events corresponding to hemozoin-laden macrophages[8] with a maximum sensitivity and specificity of 97%[22] and 98%,[23] respectively. For the Coulter analyzers, a malaria discriminant factor that uses monocyte and lymphocyte DC measurements has a maximum sensitivity and specificity of 98% and 96.9%, respectively.[4,21] More recently, using the XE-2100 analyzer, two case series in South Korea, one with 16 and one with 3 *P. vivax*-infected patients, described pseudoeosinophilia and abnormal granulocyte-coded events in the DIFF scatterplot in approximately 38% of samples.[9,10] In 2008, Huh and others[5] in South Korea compared these two findings against thick-film malaria diagnosis in 144 samples of *P. vivax*-infected patients and in 319 samples from febrile patients, reporting a sensitivity

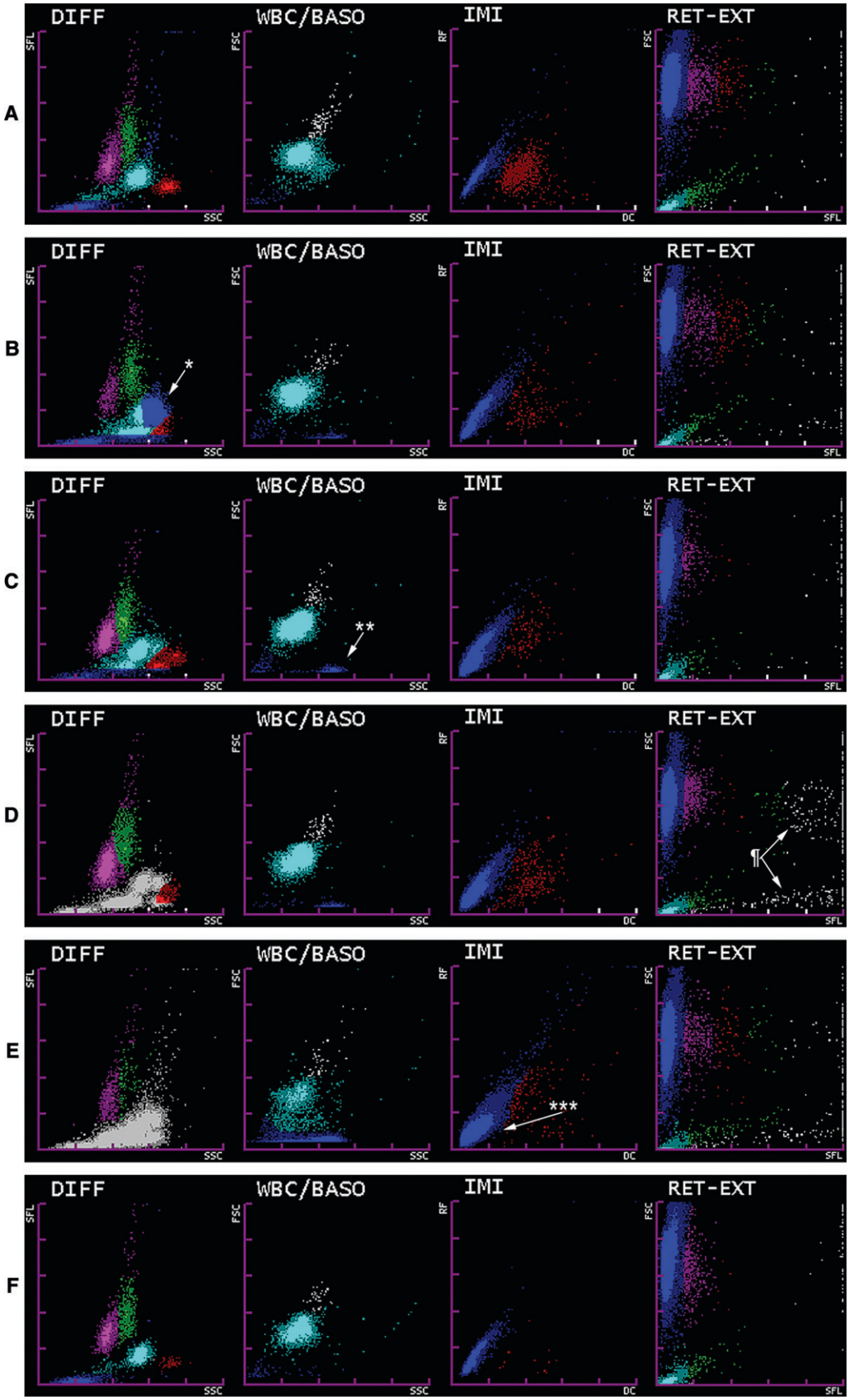

FIGURE 3. Representative scatterplots of samples from **A** (AFS group), **B–E** (*P. vivax* group), and **F** (*P. falciparum* group). **B–E** show the general XE-2100 *P. vivax* pattern. *Abnormal patterns are the granulocyte-coded events in the DIFF scatterplot. **The pixel-counting area in the WBC/BASO(III). ***The larger WBC ghost group in the IMI scatterplot. ¶The medium and low FSC linear patterns of gray-coded events in RET-EXT(V) and (VI). (**F**) Scatterplots from a *P. falciparum* sample showing the similarity with the AFS sample (**A**) and the lack of significant abnormalities.

Table 2
Diagnostic accuracy of categorized pixel counts

Scatterplot (area for pixel count) [optimal cut-off pixel count]	TP	TN	Sensitivity (95% CI)	Specificity (95% CI)
P. vivax				
DIFF(I) [8]	54/65	60/63	83.1 (73.2–93.0)	95.2 (89.2–100)
WBC/BASO(III) [7]	61/63	61/65	96.8 (91.7–100)	93.9 (87.2–100)
RET-EXT(V) [3]	48/65	52/63	73.9 (62.4–85.3)	82.5 (72.4–92.7)
RET-EXT(VI) [1]	50/65	48/63	76.9 (65.9–87.9)	76.2 (64.9–87.5)
P. falciparum				
WBC/BASO(III) [3]	18/30	42/63	60 (41–79)	67 (54–79)
DIFF(II) [7]	22/30	38/63	73 (56–91)	60 (47–73)

Scatter plot label and counting area specified by Roman numerals is shown in Figure 2, and they appear in this format throughout the text. TP = true positive; TN = true negatives.

of 69.4% and a specificity of 100%.[5] Other small case series have described similar findings[6,24] in *P. vivax* infected samples, and a case describing an elevated reticulocyte/IRF ratio and an increase in highly fluorescent lymphocyte-coded events in the DIFF scatterplot [DIFF(II) area] in a *P. falciparum*-infected patient[25] has been published by the Sysmex Corporation. In our study, we have confirmed most of these previous findings and further explored all the malaria-related abnormalities detected by the XE-2100. We have optimized the XE-2100s malaria-diagnostic capacity by building models with the best malaria-predictor variables and computed them into an optimal PP value (index test) that also enables the automation of the method. The models developed were two OD and two N-OD models for *P. vivax* and two N-OD models for *P. falciparum* that showed an accuracy above 94.7% (*P. vivax* models) and 85% (*P. falciparum* models). Validation analyses further showed that all models had similar accuracies with less than 5% variation from the original models, except for the N-OD1$_{Pf}$ that showed a 9% increment in accuracy (from 85% to 94%).

The general scatterplot XE-2100 *P. vivax* pattern (U-OD$_{Pv}$) had an accuracy of 95.3% (95% CI = 91.3–99.4%) and was further simplified to a Malaria$_{Pv}$ Score (M-OD$_{Pv}$) that improved the accuracy to 96.9% (95% CI = 93.5–100%). The observer bias associated with the OD criteria was minimized by only including variables with acceptable interrater and intrarater reproducibility (Supplementary Table 1), and the XE-2100 *P. vivax* pattern had an excellent interrater reproducibility (kappa of 0.92).[26] The study by Huh and others[5] described abnormal DIFF scatterplots in 52% of samples with *P. vivax*. Our study found that 98% of samples with *P. vivax* parasites had at least 1 of 10 DIFF abnormalities used for the M-OD$_{Pv}$. We also describe abnormalities not previously reported in the WBC/BASO, RET-EXT, and IMI scatterplots that substantially increased the description and accuracy of the XE-2100 *P. vivax* pattern. Optimal cut-off pixel counts in the DIFF(I), WBC/BASO(III), RET-EXT(V), and RET-EXT(VI) for *P. vivax* and in the WBC/BASO(III) and DIFF(II) for *P. falciparum* were accurate and objective variables that could be used to complement the OD models (Figures 2 and 3; Table 2). The pixel count in the WBC/BASO(III) area was especially important, because it is easily identifiable, had the highest diagnostic accuracy, and was retained as the strongest predictor variable in all models that used scatterplot information (OD and N-OD2; Tables 3 and 4). We found no reliable *P. falciparum* scatterplot pattern to develop an OD$_{Pf}$.

Most research done in the field of malaria diagnosis with hematology analyzers proposes observer-dependent diagnostic criteria,[20] including the study done by Huh and others[5] to evaluate the XE-2100. Malaria diagnosis with hematology analyzers could have more clinical relevance and impact on patient's care if implemented as an automated malaria alarm integrated to the XE-2100 IPU or a LIS. With this premise, we developed the N-OD models using the built-in XE-2100 variables available (N-OD1 models) and pixel counts in areas not registered by the commercial XE-2100 IPU (N-OD2 models). The N-OD models had a good overall accuracy and reproducibility on validation analyses, and the N-OD2 models were more parsimonious and accurate than the N-OD1 models when the WBC/BASO(III) pixel count was included (Tables 3 and 4). Both *P. falciparum* N-OD models were less accurate than *P. vivax* models, most likely because of fewer scatterplot abnormalities.

In all the N-OD diagnostic models, the descent in platelet count measured as plaquetocrit or PLT-O was a significant malaria predictor as expected by the thrombocytopenia caused by the disease. The continuous increment in the mean LYMPH-Y value was a good predictor variable in both N-OD1 *P. vivax* and *P. falciparum* models, and it showed a weak but significant correlation with the pixel count in DIFF(II) (area for atypical lymphocytes; Figure 1) and correlated with the presence of *P. vivax* rings and schizonts and *P. falciparum* rings (Table 5). An increase in events in the DIFF(II) had already been reported in a patient with *P. falciparum* malaria.[25] Hemozoin-laden macrophages could potentially generate a high side-scatter signal erroneously detected as SFL[27] and registered in the LYMPH-Y channel. The number of rings alone is unlikely to produce this signal, but ring parasitemia may correlate with the concentration of hemozoin-laden monocytes.[23,28] The increase in ΔDIFF/WBC was a good predictor in the N-OD1$_{Pv}$ model, and it correlated significantly with the variable number of granulocyte-coded abnormalities in the DIFF scatterplot. Both of these variables showed a significant correlation with *P. vivax* mature trophozoites (Table 5). For the *P. falciparum* N-OD$_{Pf}$ models, the variable RDW-SD, despite the lack of significant correlation, could be associated with the presence of ring forms interfering with the DC measurements, generating a wider distribution with extra peaks in the RBC histograms (Supplementary Figure 2).

Abnormal scatterplot events in Cell-Dyn analyzers are associated with the detection of hemozoin-laden macrophages.[8] However, for the XE-2100, no studies have directly explored such association. Huh and others[5] followed 24 samples post-treatment and found resolution of all DIFF scatterplot abnormalities by day 3, which coincides with the expected time for microscopic parasite negativity. We found that most of the

TABLE 3
Multivariate logistic regression predictive models for *P. vivax* and *P. falciparum*

Developed models					Validation		
Model*	Variables	β	Unadjusted DOR (95% CI)†	Adjusted DOR (95% CI)†	Model‡	β	Adjusted DOR (95% CI)†
M-OD$_{Pv}$ A: 96.9% R^2 = 0.95	≥ 7 pixels in the WBC/BASO(III)	5.931	465.13 (82.12–2634.34)	376.70 (9.78–14501.74)	A: 97.0% R^2 = 0.91	5.085	161.54 (12.43–2099.11)
	Number of granulocyte-coded DIFF abnormalities§	2.015	3.81 (2.05–7.07)	7.50 (1.57–35.81)		1.117	3.05 (1.56–5.98)
N-OD1$_{Pv}$ A: 94.7% R^2 = 0.85	ΔDIFF/WBC	0.046	1.03 (1.03–1.04)	1.05 (1.02–1.08)	A: 95.1% R^2 = 0.82	0.034	1.04 (1.01–1.05)
	Plaquetocrit	–0.205	1.27 (1.16–1.38)	1.23 (1.07–1.41)		–0.187	1.20 (1.06–1.37)
	LYMPH-Y	0.045	1.04 (1.03–1.06)	1.05 (1.02–1.08)		0.047	1.05 (1.02–1.08)
N-OD2$_{Pv}$ A: 96.8% R^2 = 0.93	PLT-O	–0.029	1.02 (1.02–1.03)	1.02 (1.00–1.05)¶	A: 96.8% R^2 = 0.92	–0.024	1.02 (1.01–1.04)
	Pixels WBC/BASO(III)	0.618	1.55 (1.24–1.93)	1.86 (1.27–2.7)		0.450	1.57 (1.23–2.00)
N-OD1$_{Pf}$ A: 85% R^2 = 0.59	PLT-O	–0.018	1.02 (1.03–1.01)	1.02 (1.01–1.03)	A: 94% R^2 = 0.59	–0.030	1.03 (1.02–1.04)
	RDW-SD	0.502	1.49 (1.22–1.81)	1.75 (1.27–2.43)		0.417	1.52 (1.13–2.04)
	LYMPH-Y	0.019	1.03 (1.01–1.04)	1.02 (1.00–1.04)‖		0.030	1.03 (1.01–1.05)
N-OD2$_{Pf}$ A: 89% R^2 = 0.64	PLT-O	–0.020	1.02 (1.01–1.03)	1.02 (1.01–1.03)	A: 94% R^2 = 0.62	–0.033	1.03 (1.02–1.05)
	RDW-SD	0.551	1.49 (1.22–1.81)	1.73 (1.30–2.30)		0.456	1.58 (1.17–2.13)
	Pixels WBC/BASO(III)	0.349	1.29 (1.08–1.53)	1.42 (1.11–1.82)		0.336	1.40 (1.14–1.72)

Model validation samples: total (N = 218), *P. vivax* (N = 39), *P. falciparum* (N = 18), and compound control group (N = 161). Sample size for each validation analysis: M-OD$_{Pv}$ (N = 200), N-OD1$_{Pv}$ (N = 182), N-OD2$_{Pv}$ (N = 190), and N-OD1$_{Pf}$ and N-OD2$_{Pf}$ (N = 168). β$_0$ for each build model/validation model: M-OD$_{Pv}$ –6.559/–5.941, N-OD1$_{Pv}$ –74.130/–63.945, N-OD2$_{Pv}$ 0.328/–0.129, N-OD1$_{Pf}$ –31.024/–33.051, and N-OD2$_{Pf}$ –21.351/–15.869. Hosmer–Lemeshow goodness-of-fit P values for built models: M-OD$_{Pv}$ = 0.95, N-OD1$_{Pv}$ = 0.95, N-OD2$_{Pv}$ = 0.94, N-OD1$_{Pf}$ = 0.82, and N-OD2$_{Pf}$ = 0.26. More information on model fit, accuracy, and validation is given in Supplementary Panel 2.

* Model's code A, model's accuracy; Nagelkerkes R^2, model's coefficient of determination.

† For negative β coefficients, the DOR odds ratios are expressed as reciprocals (increased probability).

‡ Partial cross-validation analyses with Nagelkerkes R^2 and model's accuracy.

§ Ten possible abnormalities shown in Figure 2.

¶ P = 0.012.

‖ P = 0.041.

abnormalities in the DIFF, WBC/BASO, and RET-EXT scatterplots correlated significantly with the concentration of *P. vivax* mature trophozoites, schizonts, and gametocytes (Table 5; Supplementary Table 4). Additionally, the scatterplot localization of malaria-related events coincides with the expected patterns for mature trophozoites (Table 5; Figures 2 and 3): In the DIFF scatterplot, events with high SSC values in the granulocyte area are compatible with signals generated by hemozoin-containing mature forms that could also generate a nucleic acid-derived SFL signal toward the DIFF(I) area. For the WBC/BASO(III) events, the SSC values similar to basophils combined with the low FSC values are compatible with signals generated by hemozoin-containing corpuscles smaller than a WBC such as mature trophozoites and schizonts. We did not find a significant increase in the reticulocyte/IRF ratio as reported previously (Supplementary Table 2).[25] However, the RET-EXT scatterplot of *P. vivax* samples showed highly fluorescent (SFL), gray-coded events distributed in linear or clustered patterns, which could correspond to the parasite's nucleic acid or hemozoin, with size ranges (FSC) between RBCs (RET-EXT(V)) or platelets [RET-EXT(VI); Figures 2 and 3]. These events showed significant correlation with gametocyte, schizont, and mature trophozoite parasitemia. The virtual lack of scatterplot abnormalities in the *P. falciparum* samples, containing mainly rings, further supports the hypothesis that most abnormalities detected by the XE-2100 correspond to mature parasites, as found in *P. vivax* malaria. Despite the sequestering of mature *P. falciparum* parasites and the resulting few scatterplot abnormalities, this species was accurately detected by the N-OD1$_{Pf}$ variable combination of RDW-SD, PLT-O, and LYMPH-Y. Research specifically tailored to establish the cause of all abnormalities (i.e., by analyzing parasite-synchronized samples with an open XE-2100 flow cytometer) is still needed.

Pseudoeosinophilia has been reported as a common finding in XE-2100 blood analyses performed in *P. vivax*-infected samples.[5,9] Huh and others[5] found that ≥ 5% pseudoeosinophilia in *P. vivax*-infected samples had a sensitivity of 38.9% and a specificity of 100%. We found that the optimal *P. vivax*-diagnostic pseudoeosinophilia was 20.9% and had an accuracy of 60.5% (95% CI = 51.1–69.9%). However, this diagnostic criterion requires microscopic blood evaluation and a manual calculation, limiting its applicability in clinical scenarios. Regarding the malaria detection threshold for the XE-2100, Huh and others[5] found that the sensitivity increased from 39.3% to 88.6% in samples with more 500 parasites/μL,[5] and in our study, the *P. vivax* sample with the lowest parasitemia (190 parasites/μL) was detected by both N-OD$_{Pv}$ models.

A two-gate case-control design was chosen to optimize the construction of diagnostic models where the dependent variable (malaria status) needed to be known before performing accuracy analyses. This type of sampling precludes population-based inferences (diagnostic predictive values), potentially limiting external validity, and may overestimate the diagnostic accuracy of the index test, because the samples used to develop the models were also used to test their diagnostic accuracy. To assess the external validity of the built models, a partial-validation procedure was performed. The regression parameters, accuracy, and Youden's J were consistent with the estimates obtained for the original models, especially when accuracy was compared, because the PPs tended to pool toward extreme values (PP ≈ 0.0 or 1.0) where small variations in the regression

TABLE 4
Accuracy of diagnostic models developed for *P. vivax* and *P. falciparum*

Criteria	TP	TN	Sensitivity (95% CI)	Specificity (95% CI)	LR+ (95% CI)	LR– (95% CI)	Youden's *J* (95% CI)	Youden's *J** (95% CI)
U-OD$_{Pv}$	63/65	59/63	96.9 (92.0–100)	93.6 (86.8–100)	15.27 (5.91–39.45)	0.03 (0.01–0.13)	0.91 (0.83–0.98)	0.93 (0.87–0.99)
M-OD$_{Pv}$†	62/65	62/63	95.4 (89.5–100)	98.4 (94.5–100)	60.09 (8.59–420.30)	0.05 (0.02–0.14)	0.94 (0.88–1.00)	0.93 (0.86–1.00)
N-OD1$_{Pv}$	50/53	58/61	94.3 (87.2–100)	95.1 (88.8–100)	19.18 (6.35–57.94)	0.06 (0.02–0.18)	0.89 (0.81–0.98)	0.88 (0.77–0.98)
N-OD2$_{Pv}$	61/63	61/63	96.8 (91.7–100)	96.8 (91.7–100)	30.50 (7.79–119.37)	0.03 (0.01–0.13)	0.94 (0.88–1.00)	0.93 (0.86–1.00)
N-OD1$_{Pf}$	26/28	51/63	93 (82–100)	81 (71–91)	4.88 (2.90–8.20)	0.09 (0.02–0.34)	0.74 (0.60–0.87)	0.78 (0.66–0.91)
N-OD2$_{Pf}$	24/28	57/63	86 (71–100)	90 (82–99)	9.00 (4.14–19.55)	0.16 (0.06–0.39)	0.76 (0.61–0.91)	0.83 (0.67–0.99)

TP = true positives; TN = true negatives.
* Results for validation sample: total (N = 218), *P. vivax* (N = 39), *P. falciparum* (N = 18), and compound control group (N = 161).
† For M-OD$_{Pv}$ (original coefficients) cut-off PP = 0.59 (ROC AUC 0.996; $P < 0.001$) and for malaria$_{Pv}$ score (shown in table) cut-off PP = 0.56 (≥ 4 points; ROC AUC 0.996; $P < 0.001$; Supplementary Figure 3). For the N-OD1$_{Pv}$ cut-off PP = 0.42 (ROC AUC 0.975; $P < 0.001$), and for N-OD2$_{Pv}$ cut-off PP = 0.42 (ROC AUC 0.993; $P < 0.001$). For N-OD1$_{Pf}$ cut-off PP = 0.29 (ROC AUC 0.916; $P < 0.001$), and for N-OD2$_{Pf}$ cut-off, PP = 0.37 (ROC AUC 0.921; $P < 0.001$).

coefficients had little impact on the model's accuracy (Tables 3 and 4; Supplementary Panel 2).[29] Performance of the N-OD1 models in clinical scenarios where hematologic pathologies could potentially interfere with the LYMPH-Y and ΔDIFF/WBC measurements is uncertain; however, the combination of several parameters to achieve a robust PP diagnostic criterion could give some stability to the models. The time to process the samples was outside routine practice, but it conforms to the sample viability frame.[15] More importantly, the time was similar between groups, suggesting that any small variation was symmetrically distributed, and the models were not significantly altered by this factor.

Health personnel with access to automated FBCs should become familiar with the OD malaria-associated findings. Malaria diagnosis with hematology analyzers, as we have shown for the XE-2100, could become an important failsafe tool in scenarios where clinicians and laboratory personnel are less likely to suspect and test for malaria. In Hungary, a patient not suspected of having malaria was later diagnosed with a mixed *P. vivax* and *P. malariae* infection based on an OD$_{Pv}$ finding—an extra neutrophil-coded group in the DIFF scatterplot.[24] Thrombocytopenia, anemia, and the presence of a general XE-2100 *P. vivax* pattern (U-OD$_{Pv}$) or a positive Malaria$_{Pv}$ Score (M-OD$_{Pv}$) in a febrile patient should prompt a microscopic analysis for *P. vivax* malaria, whereas the presence of thrombocytopenia, anemia, and pixel counts in WBC/BASO(III) and DIFF(II) (Table 2) could be used to rule out *P. falciparum* malaria.

The N-OD1 diagnostic models can provide the framework for the development of malaria alarms for commercial XE-2100 analyzers currently operating. The PP equation for both N-OD1$_{Pv}$ and N-OD1$_{pf}$ models (Table 3) can be automatically computed with each patient's variable values using a LIS and the detection threshold set at the optimal PPs given in Table 4 (Supplementary Example, available at www.ajtmh.org). Scatterplot abnormalities seen in the images produced by the IPU correspond to a limited fraction of events detected by the XE-2100s flow cytometer, but these were significant enough to allow for a reproducible analysis and be accurate predictors of malaria. The N-OD2 diagnostic models provide new scatterplot variables like the pixel counts in WBC/BASO(III), RET-EXT(V), and RET-EXT(VI), that could potentially be used by the industry to improve the prediction algorithm and incorporate it into the XE-2100 IPU.

Finally, malaria detection with modern hematology analyzers could be optimized by calibrating the instruments to detect blood abnormalities associated with malaria. Experimental malaria-cytometry studies have found a detection threshold of 50 parasites/μL.[30] Furthermore, in a study using a Sysmex SIF flow cytometer, the authors were able to differentiate *P. falciparum* parasite stages based on fluorescence patterns,[31] providing evidence for the potential for improving malaria detection with commercial flow cytometers, including the XE-2100. Our findings, specially the N-OD2 models, suggest that the XE-2100 could become an accurate tool for malaria diagnosis, allowing for a timely microscopic blood evaluation of affected patients.

TABLE 5
Association between XE-2100 variables and parasite counts for each *Plasmodium* species

Variable	R^2	*P* values correspond to the linear regression coefficients			
		Rings	Mature trophozoites	Schizonts	Gametocytes
P. vivax					
Number of granulocyte-coded DIFF abnormalities*	0.365	0.274	< 0.001†	0.474	0.103
ΔDIFF/WBC	0.501	0.587	< 0.001†	0.645	0.538
LYMPH-Y	0.206	0.011†	0.170	0.016†	0.813
DIFF(I)	0.602	0.027†	< 0.001†	0.029†	0.648
WBC/BASO(III)	0.408	0.160	< 0.001†	0.030†	0.648
RET-EXT(V)	0.545	0.788	< 0.001†	0.021†	0.045†
RET-EXT(VI)	0.586	0.679	< 0.001†	0.951	0.805
P. falciparum					
LYMPH-Y	0.305	0.036†	–	–	0.182
DIFF(I)	0.928	0.064‡	–	–	< 0.001†
WBC/BASO(III)	0.073	0.545	–	–	0.347

* Ten categorical variables shown in Figure 2.
† Marginally non-significant *P* value for regression coefficient.
‡ Significant regression coefficient.
Regression coefficients and additional variables can be found in Supplementary Table 4.

Received August 10, 2009. Accepted for publication December 15, 2009.

Note: Supplementary materials appear at www.ajtmh.org.

Acknowledgments: The authors thank the staff of the participating health centers, especially Rosa Porto, Ana Rosa Rodríguez, Cruz María Gómez, Mario Sibaja, Dr. Orlando Pontón, and José Ignacio Coa at the Hospital San Sebastián de Urabá in Necoclí, Jaime Quiñones at the Hospital San Rafael in Zaragoza, Dania Vídez at the Hospital Nuestra Señora del Carmen in El Bagre, and Dr. Felipe Sanín and Fernando Mendez from the Grupo Malaria at Turbo. The authors also thank the informatics department at the Laboratorio Clínico Hematológico. Diana Fernández, Cecilia Giraldo, and Ana María Vásquez of the Grupo Malaria performed duplicate microscopy. We also thank Ana Isabel Toro and César Segura for reviewing the final manuscript. Finally, the authors thank all patients and participants.

Financial support: This study was funded by the Laboratorio Clínico Hematológico S.A. Medellín, Colombia and the Grupo Malaria, Universidad de Antioquia, Medellín, Colombia.

Disclosure: Some of the authors wish to disclose that they have received technical support (two consultancies) from the Sysmex Corporation regarding this project in relation to accessing the hematology analyzer's technical variable database. No direct funding or benefits such as trips, conference participations, or commercial contracts have been offered or received by Sysmex Corporation regarding the research presented in the submitted paper. This statement is made in the interest of full disclosure and not because the authors consider this to be a conflict of interest.

Authors' addresses: Germán Campuzano-Zuluaga, Gonzalo Álvarez-Sánchez, Alexandra Marcela Ríos-Orrego, Adriana Pabón-Vidal, Andrés Felipe Miranda-Arboleda, and Silvia Blair-Trujillo, Grupo Malaria, Universidad de Antioquia, Medellín, Colombia, E-mails: germancz81@gmail.com, gonzalv@quimbaya.udea.edu.co, alexrioso@hotmail.com, apabon72@gmail.com, mirandaarboleda@gmail.com, and sblair@quimbaya.udea.edu.co. Germán Campuzano-Zuluaga, Gloria Elcy Escobar-Gallo, Luz Marina Valencia-Zuluaga, and Germán Campuzano-Maya, Laboratorio Clínico Hematológico, Medellín, Colombia, E-mails: germancz81@gmail.com, lablch@hematologico.com, comunicaciones@hematologico.com, and gcampuzano@hematologico.com.

Reprint requests: Germán Campuzano-Zuluaga, Laboratorio Clínico Hematológico, Carrera 43C No. 5-33, Medellín, Colombia 050022, E-mail: germancz81@gmail.com.

REFERENCES

1. Newman RD, Parise ME, Barber AM, Steketee RW, 2004. Malaria-related deaths among U.S. travelers, 1963–2001. *Ann Intern Med 141:* 547–555.
2. Lema OE, Carter JY, Nagelkerke N, Wangai MW, Kitenge P, Gikunda SM, Arube PA, Munafu CG, Materu SF, Adhiambo CA, Mukunza HK, 1999. Comparison of five methods of malaria detection in the outpatient setting. *Am J Trop Med Hyg 60:* 177–182.
3. Mendelow BV, Lyons C, Nhlangothi P, Tana M, Munster M, Wypkema E, Liebowitz L, Marshall L, Scott S, Coetzer TL, 1999. Automated malaria detection by depolarization of laser light. *Br J Haematol 104:* 499–503.
4. Fourcade C, Casbas MJ, Belaouni H, Gonzalez JJ, Garcia PJ, Pepio MA, 2004. Automated detection of malaria by means of the haematology analyser Coulter GEN.S. *Clin Lab Haematol 26:* 367–372.
5. Huh HJ, Oh GY, Huh JW, Chae SL, 2008. Malaria detection with the Sysmex XE-2100 hematology analyzer using pseudoeosinophilia and abnormal WBC scattergram. *Ann Hematol 87:* 755–759.
6. Yan F, Dai Y, Zhang Z, Wan H, 2008. The correlation of abnormal information in Sysmex hematology analyzers XE-2100 and XS-1000*i* with diagnosis of *Plasmodium* infection. *Sysmex Journal International 18:* 50–53.
7. Walters J, Garrity P, 2000. Performance evaluation of the Sysmex XE-2100 hematology analyser. *Lab Hematol 6:* 83–92.
8. Grobusch MP, Hanscheid T, Kramer B, Neukammer J, May J, Seybold J, Kun JF, Suttorp N, 2003. Sensitivity of hemozoin detection by automated flow cytometry in non- and semi-immune malaria patients. *Cytometry B Clin Cytom 55:* 46–51.
9. Huh J, Jung J, Yoon H, Chung W, 2005. Pseudoeosinophilia associated with malaria infection determined in the Sysmex XE-2100 hematology analyzer. *Ann Hematol 84:* 400–402.
10. Park GB, Cha YJ, 2006. Three cases of pseudoeosinophilia associated with malaria determined in the Sysmex XE-2100 automated hematology analyzer. *Korean J Lab Med 26:* 77–80.
11. Dirección Seccional de Salud de Antioquia, 2006. *Events of Public Health Interest—Antioquia 2006*. Available at: http://www.dssa.gov.co/htm/event_1.html. Accessed November 1, 2008.
12. Rutjes AW, Reitsma JB, Vandenbroucke JP, Glas AS, Bossuyt PM, 2005. Case-control and two-gate designs in diagnostic accuracy studies. *Clin Chem 51:* 1335–1341.
13. Peduzzi P, Concato J, Kemper E, Holford TR, Feinstein AR, 1996. A simulation study of the number of events per variable in logistic regression analysis. *J Clin Epidemiol 49:* 1373–1379.
14. Bain B, Chiodini P, England J, Bailey J, 1997. The laboratory diagnosis of malaria. *Clin Lab Haematol 19:* 165–170.
15. Garvey B, Mahon A, McTaggart P, Parker-Williams J, 2003. *MHRA Evaluation: Sysmex XE-2100 Haematology Analyser*. Norwich, United Kingdom: Crown.
16. Matsumoto H, 1999. The technology of reagents in the automated hematology analyzer Sysmex XE-2100™—red fluorescence reaction. *Sysmex Journal International 9:* 179–185.
17. Ruzicka K, Veitl M, Thalhammer-Scherrer R, Schwarzinger I, 2001. The new hematology analyzer Sysmex XE-2100: performance evaluation of a novel white blood cell differential technology. *Arch Pathol Lab Med 125:* 391–396.
18. Kumar A, Yerneni LK, 2009. Semi-automated relative quantification of cell culture contamination with mycoplasma by Photoshop-based image analysis on immunofluorescence preparations. *Biologicals 37:* 55–60.
19. Landis JR, Koch GG, 1977. The measurement of observer agreement for categorical data. *Biometrics 33:* 159–174.
20. Hanscheid T, Valadas E, Grobusch MP, 2000. Automated malaria diagnosis using pigment detection. *Parasitol Today 16:* 549–551.
21. Briggs C, Da Costa A, Freeman L, Aucamp I, Ngubeni B, Machin SJ, 2006. Development of an automated malaria discriminant factor using VCS technology. *Am J Clin Pathol 126:* 691–698.
22. Hanscheid T, Langin M, Lell B, Potschke M, Oyakhirome S, Kremsner PG, Grobusch MP, 2008. Full blood count and haemozoin-containing leukocytes in children with malaria: diagnostic value and association with disease severity. *Malar J 7:* 109.
23. Padial MM, Subirats M, Puente S, Lago M, Crespo S, Palacios G, Baquero M, 2005. Sensitivity of laser light depolarization analysis for detection of malaria in blood samples. *J Med Microbiol 54:* 449–452.
24. Pinter E, Szabo O, Tdorova R, Varnai Z, Banhegyi D, 2007. Relapse of *Plasmodium vivax* and recrudescence of *Plasmodium malariae* malaria as detects by Sysmex XE 2100 fully automated blood cell analyzer. *Sysmex Journal International 17:* 102–105.
25. Rowan RM, Linssen J, 2005. A picture is worth a thousand words: XE-2100 and *falciparum* malaria. *Sysmex Journal International 15:* 27–38.
26. Landis JR, Koch GG, 1977. An application of hierarchical kappa-type statistics in the assessment of majority agreement among multiple observers. *Biometrics 33:* 363–374.
27. Sysmex Corporation, 2006. *Fluorescence Differentiation Supports Malaria Diagnosis*. Sysmex Europe GMBH, Norderstedt, Germany. 1–11.
28. Nguyen PH, Day N, Pram TD, Ferguson DJ, White NJ, 1995. Intraleucocytic malaria pigment and prognosis in severe malaria. *Trans R Soc Trop Med Hyg 89:* 200–204.
29. Hosmer DW, Lemeshow S, 2000. Assessing the fit of the model. Hosmer DW, Lemeshow S, eds. *Applied Logistic Regression*. New York: Wiley-Interscience Publication, 160–163.
30. van Vianen PH, van Engen A, Thaithong S, van der Keur M, Tanke HJ, van der Kaay HJ, Mons B, Janse CJ, 1993. Flow cytometric screening of blood samples for malaria parasites. *Cytometry 14:* 276–280.
31. Saito-Ito A, Akai Y, He S, Kimura M, Kawabata M, 2001. A rapid, simple and sensitive flow cytometric system for detection of *Plasmodium falciparum*. *Parasitol Int 50:* 249–257.